

# Synthesis of PET-Magnesium Oxide-Chitosan Nanocomposite Membranes for the Dehydration of Natural Gas

Oluranti Agboola<sup>1\*</sup>, Grace Ayomide Oginni<sup>1</sup>, Olagoke Oladokun<sup>1</sup>, Vincent Efevbokhan<sup>1</sup>, Augustine Omoniye Ayeni<sup>1</sup>, Ayodeji Ayoola<sup>1</sup>, Adedayo Adeyanju Adedamola<sup>1</sup>, Edith Egbinhanlu Alagbe<sup>1</sup>, Ojo Sunday Isaac Fayomi<sup>2</sup>, Lucey Moropeng<sup>3</sup>, Stephen Kehinde Ogunlade<sup>1</sup>

<sup>1</sup> Department of Chemical Engineering, College of Engineering, Covenant University, Km 10 Idiroko Road, 112104 Ota, Nigeria

<sup>2</sup> Department of Mechanical and Biomedical Engineering, Bells University of Technology, Km 8 Idiroko Road, 112104 Ota, Nigeria

<sup>3</sup> Department of Chemical, Materials and Metallurgical Engineering, Tshwane University of Technology, P. O. B. X680, 0001 Pretoria, South Africa

\* Corresponding author, e-mail: [funmi2406@gmail.com](mailto:funmi2406@gmail.com)

Received: 05 July 2022, Accepted: 03 January 2023, Published online: 27 March 2023

## Abstract

Flat thin-film magnesium oxide-chitosan nanocomposite membranes were synthesized with polyethylene terephthalate (PET) and employed for natural gas dehydration. The water vapor permeation was most pronounced with a nanocomposite membrane doped with 0.9 g MgO nanoparticles (NP) as a result of a significant upsurge in the permeability of water vapor in the membrane (0.87). With the increase in MgO NP, large macro-voids are created, substratum pore size, and thickness together with the water vapor permeation were upsurged. The dehydration of natural gas performance of magnesium oxide-chitosan nanocomposite membranes synthesized with PET was enhanced with the increase in MgO NP embedded in the membrane. Though water vapor permeation was restricted by the polyester non-woven material used as a support for the nano composite membranes, as the three membranes did not reach the permeation coefficient of 1. However, the permeation coefficient increased with an increased MgO NP, with three membrane samples (M1, M2 and M3) having permeation coefficient of 0.763, 0.77 and 0.87 respectively. The gas reduced with an increase MgO NP, with M1, M2 and M3 having  $3.46 \times 10^{-2}$ ,  $3.17 \times 10^{-2}$  and  $3.88 \times 10^{-3}$  kg/m<sup>3</sup> respectively. From the adsorption study, the discrepancy observed between CH<sub>4</sub> and vapor with isotherm models was ascribed to the different adsorption behavior of CH<sub>4</sub> and vapor on the membrane-active area. The cost of making the membrane cannot be considered as a terminal criterion because most of the cost-effective option is not always the optimum one. The membranes confirmed their suitability for the dehydration of natural gas.

## Keywords

natural gas, dehydration, nanocomposite membranes, permeability, adsorption isotherm models

## 1 Introduction

As the country's petroleum industry moves steadily from mostly exploring and producing crude oil to exploring and producing oil and gas, more concentration is being assigned to natural gas engineering projects [1]. The resources of energy like coal gas, natural gas and landfill gas (methane, ethane and ethylene, etc.) are typically found diluted with nitrogen gas and/or carbon dioxide [2]. Usually, natural gas comprises of a substantial quantity of water vapor. Alterations in temperature and pressure condense this water vapor, thereby changing the physical state from gas to liquid and then to solid. There must be a process to remove this water for the purpose of protecting the system from corrosion and hydrate development [3]. Hence, all natural gas

must be dried before it goes into the national distribution pipelines, for the purpose of controlling corrosion and averting the development of solid hydrocarbon/water hydrates [4].

The dehydration of natural gas is a subject that one cannot in any way ignore in processing the gas to consumer specifications. Presently, glycol dehydration (which is the traditional dehydration technique employed in Nigeria) possess some related problem; such as the venting of pollutants like methane, volatile organic compounds (VOCs) such as toluene, benzene, ethylbenzene, and xylenes (BTEX), from the raw natural gas streams, and hazardous air pollutants (HAPs) [1]. Particularly, benzene is known to be a carcinogen. For instance, a usual glycol-based unit dehydrating

a 55795.34 Nm<sup>3</sup>/h natural gas stream will discharge more than 40 tons per year of various organic pollutants, of which about half comprises BTEX [5]. Based on the latest estimates by EIA, 45.312 billion m<sup>3</sup> of dry natural gas is being produced in Nigeria, in 2019 [6]. It is envisaged that the emissions of organic pollutants from dehydrators in Nigeria will run into thousands of tons. Hence, controlling the emissions of these organic pollutants to have clean air in a country like Nigeria is one of the major environmental challenges confronting the natural gas industry in the country. All these glitches institute an environmental menace together with the loss of treasured gas that could be sold to make income [1]. Another disadvantage of glycol dehydration is the complex system operation that needs solvent storage, replacement and disposal [4].

Membrane technology is an interesting substitute for the dehydration of natural gas. Where feed or recycle compression is employed, the membrane system removes water as a liquid with basically zero air emissions contrasted to the glycol absorption which removes water as a vapor [7]. Usually, membrane systems are compact with a slight footprint, passive devoid of moving parts, and dependable devoid of the necessity for continuous consideration when functioning in secluded areas [4]. Membranes have been commonly adopted as a processing unit in gas separations for over 30 years. The application of membranes for natural gas dehydration began ten years ago, and these systems remain in the early stages of commercialization. Hence, there seem to be a few membrane natural gas dehydration systems currently accessible and there is not much in the literature for dehydration of natural gas using membrane technology.

Nanocomposite membranes synthesis is for the conservation of the advantages polymeric membranes possessed. This is done for the purpose of attaining a remarkably predicted outcome for membrane advancement via the incorporation of engineered nanoscale materials in membranes made from polymer [8]. Lin et al. [4] examined the methodological viability of membrane technology for the dehydration of natural gas. With specific emphasis, they focused on the laboratory-scale tests of composite membranes made from Hydrophilic microphase-separated block copolymers (Pebax®). They observed that increase in sweep gas flow rate on the permeate side of the membrane resulted in a decrease in the whole membrane transport resistance to water vapor, in consequence, upsurging water vapor permeance ( $1.5 \times 10^{-2} \text{ cm}^3/\text{m}^2 \times \text{s} \times \text{MPa}$ ). Lin et al. [9] presented a field test of Pebax®-based membranes at a natural gas processing plant and the membrane process was designed to exploit the membrane separation efficacy. The water flux

attained close to 80% of the value computed with the process simulation software for a perfect sweep/counter-current module, confirming the appropriateness of the spiral-wound modules with counter-current configuration for natural gas dehydration. Hafani et al. [10] recently prepared polyethylene terephthalate (PET)-based membranes by employing poly (ethylene glycol) (PEG) average Mn 6000 as a polymeric additive. Based on the results attained, the dehydration performance of PET membranes was improved by PEG addition. Here, PET bottles were made into flat thin-film membranes doped with magnesium oxide/chitosan for dehydration of natural gas. The morphology and water permeation across the synthesized PET membranes doped magnesium oxide/chitosan were investigated.

What informed the choice of the materials used for synthesizing PET membranes doped with magnesium oxide/chitosan are (1) recycling PET waste into valuable resources will aid in reducing its environmental impact on the planet; hence, the use of plastic bottles (2) Magnesium oxide nanoparticle was used because of its superior surface reactivity, chemical and thermal stability [11] and (3) chitosan has been found to regulate permeation enhancement to a greater extent [12]. Different researchers have examined the effect of different additives on the morphological structure of membranes for their performances. The hydrophilic structure of membrane has been attained by the addition of additives like poly ethylene oxide, glycerol and zinc chloride [13]. Polyvinylpyrrolidone (PVP) is the most commonly used additive for membrane modification [14]. Different additives serve different roles in membrane preparation; however, PEG possess the same role as PVP in membrane formation [15], PEG acts as a macrovoid formation barrier and increases membrane hydrophilicity [16].

## 2 Materials and methods

Materials used for the study are deionized water, magnesium nitrate hexahydrate ( $\text{MgNO}_3 \times 6\text{H}_2\text{O}$ ), sodium hydroxide (NaOH), trifluoroacetic acid (TFA), dichloromethane (DCM), poly(ethyleneglycol) (PEG), chitosan powder, PET bottles, polyester non-woven material, ethanol, natural gas in a compressed natural gas cylinder. All reagents used for this study are analytical grade reagents and are suitable for a variety of analytical techniques.

### 2.1 Synthesis of magnesium oxide nanoparticle

Magnesium oxide nanoparticles were synthesized by sol-gel procedure by employing magnesium nitrate as a precursor [17]. 0.2 M magnesium nitrate was prepared by dissolving 2.97 g of solid magnesium nitrate in 100 mL of

deionized water and 0.5 M of sodium hydroxide NaOH was prepared by dissolving 2 g in 100 mL of deionized water. 90 mL of the 0.2 M of magnesium nitrate was measured and poured into a beaker and 10 mL of the 0.5 M of sodium hydroxide NaOH was measured and added dropwise (10 drops/2 min) to the already measured solution of magnesium nitrate at an interval 2 min while the mixture was still being stirred with a magnetic stirrer. The stirring was carried out for 30 min and afterward, a pH of 9 was attained. The supernatant was decanted off and the precipitate was poured into a crucible and placed in an oven for 180 min at 300 °C. The resulting dried white powder samples were scrapped into a sample bottle and weighed.

## 2.2 Preparation of PET

Used PET bottles were rinsed with distilled water to remove dirt and then cut with scissors into shreds readily available for recycling. The shredded material was melted to molten and then crushed into sizable beads by means of an electrical crusher. The sizable PET beads were processed to powdery nano-size polymer using a mechanical grinder. An industrial sieve shaker was employed for sieving crushed material off the desired particle size of 100 µm.

## 2.3 Synthesis of chitosan doped magnesium oxide nanocomposite membranes

Three membrane samples were synthesized according to De Silva [18]. 7 g of crushed waste PET, 2 g PEG, chitosan powder in the range of 0.1 to 0.7 g and MgO nanoparticle in the range of 0.3 to 0.9 g were weighed and placed in an Erlenmeyer flask. 20 mL of TFA and 40 mL of DCM in a ratio of 1:2 was measured and added into a beaker, the resulting mixture was stirred on a magnetic stirrer. At 2 min interval, the polymer and the additives were added in small quantities into the solvent mixture getting stirred till it got exhausted for 1 h. The resulting viscous solution was casted on the casting plate with the use of a casting knife on a polyester non-woven material. Then the plate was placed into a bath containing ethanol for 90 secs before it was removed from it and left to evaporate. The membrane was formed. Other membranes were prepared with the 0.6 g of MgO and 0.9 g of MgO to study the efficiency of the nanocomposite membranes. The membrane nanocomposite synthesis design is shown in Table 1.

## 2.4 Dehydration of natural gas procedure

The wet gas stream was obtained from Nigerian Petroleum Development Company at pressure a pressure 52 Barg and temperature of 35.63 °C. The composition of the gas is

**Table 1** Membrane nanocomposite synthesis design

Membrane samples	Amount of PET (g)	Amount of chitosan (g)	Amount of PEG (g)	Amount of MgO NPs (g)
M1	7.0	0.7	2.0	0.3
M2	7.0	0.4	2.0	0.6
M3	7.0	0.1	2.0	0.9

**Table 2** Composition of natural gas sample before dehydration

Components	Composition (mol%)
CH <sub>4</sub>	81.2%
CO <sub>2</sub>	2%
Water vapour	1.1%
C <sub>2</sub> H <sub>6</sub>	9.76%
C <sub>3</sub> H <sub>8</sub>	2.7%
C <sub>4</sub> H <sub>10</sub>	0.8%
C <sub>5</sub> H <sub>12</sub>	2.23%
C <sub>6</sub> H <sub>14</sub>	0.11%
C <sub>7</sub> H <sub>16</sub>	0.05%
C <sub>8</sub> H <sub>18</sub>	0.02%
N <sub>2</sub>	0.03%

shown in Table 2. The composite membrane was placed in the membrane cell. The well head gas was in a cylinder and it was connected to the membrane cell inlet. The ball valve attached to the equipment inlet was opened to enable the passage of gas through and into the cell. The schematic representation of the membrane cell is depicted in Fig. 1. The flowrate was measured and used to calculate the permeation. After 20 min, the retained gas was collected in a bicycle tube and analyzed with a gas analyzer.

## 2.5 Characterization

The morphological structure of the MgO nanoparticle and of the fabricated composite membranes were studied by employing scanning electron microscopy (SEM) with Energy Dispersive Spectroscopy (EDS) and X-ray diffraction (XRD).

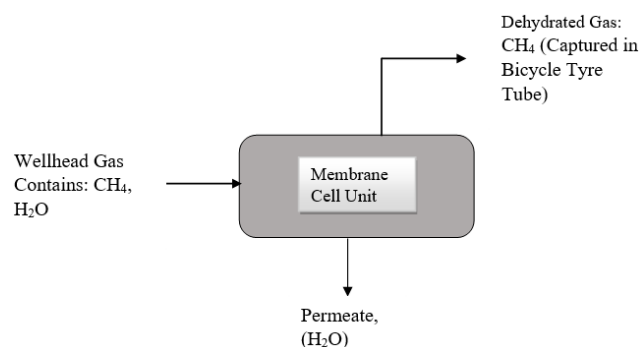


**Fig. 1** Representation illustrating the natural gas dehydration membrane cell unit

## 2.6 Membrane performance

The synthesized nanocomposite membranes were cut into a disk shape for the gas dehydration cell with a thickness in the range of  $1.9398 \times 10^{-7}$  m,  $1.9504 \times 10^{-7}$  nm and  $1.9716 \times 10^{-7}$  nm, a 0.005 m strip allowance was allowed on the edges of the cell for the purpose of achieving the membrane sealing, an active area of  $0.009505 \text{ m}^2$  was attained. The permeance of water vapor was computed from the following equations. The permeation rate is given by Eq. (1) and the water vapor permeability of the membranes was studied using Eq. (2):

$$Q_{vap} = AJ_{vap}(P_f X - P_p Y), \quad (1)$$

$$J_{vap} = \frac{Q_{vap}}{A(P_f X - P_p Y)}, \quad (2)$$

where  $Q_{vap}$  is the permeation rate ( $\text{cm}^3/\text{s}$ ) of the water vapor,  $J_{vap}$  is the permeance of water vapor ( $\text{cm}^3/\text{m}^2 \times \text{s} \times \text{MPa}$ ),  $A$  is the effective membrane area for permeation ( $\text{m}^2$ ),  $X$  and  $Y$  are respectively, the concentrations of feed side water vapor and permeate side water vapor. The feed and permeate pressures are represented by  $P_f$  and  $P_p$  in (Hgmm) [19].

Three different adsorption studies were done to study the performance of the membranes. Langmuir adsorption which was primarily designed to describe gas-solid phase adsorption was used to study the performance of the membranes by quantifying and contrasting the adsorptive capacity of the gas adsorbents [20]. The Langmuir isotherm is given by Eq. (3) [21–23]:

$$\frac{C_e}{q_e} = \frac{1}{q_m k_e} + \frac{C_e}{q_m}. \quad (3)$$

Here,  $C_e$  is concentration of adsorbate at equilibrium (mg/g).  $K_L$  is Langmuir constant related to adsorption capacity (mg/g), which can be connected with the difference of the appropriate area and porosity of the adsorbent. Therefore, adsorption capacity is given by Eq. (4):

$$q_t = (C_0 - C_t) \frac{V}{W}, \quad (4)$$

where  $q_t$  is the amount of species adsorbed per gram (or volume) of an adsorbent at any time  $t$ ,  $C_0$  (mg/L) and  $C_t$  (mg/L) are adsorbate concentrations at initial and at time  $t$ ,  $V$  (L) and  $W$  (g) are respectively the volume of the solution and the weight of the adsorbent. Fowler-Guggenheim isotherm in Eq. (5) was also studied to take the lateral interaction of the adsorbed molecules into consideration:

$$\ln \left[ \frac{C_e (1 - \theta)}{\theta} \right] = \ln K_{FG} + \frac{2w\theta}{RT}, \quad (5)$$

where  $K_{FG}$  is Fowler-Guggenheim equilibrium constant (Lm/g),  $\theta$  is fractional coverage,  $R$  is universal gas constant (kJ/mol K),  $T$  is temperature ( $^{\circ}\text{C}$ ), and  $w$  is interaction energy between adsorbed molecules (kJ/mol). Finally, the Hill-de Boer (Eq. (6)) isotherm model was used to describe a moveable adsorption together with lateral interaction among adsorbed molecules [24]:

$$\ln \left[ \frac{C_e (1 - \theta)}{\theta} \right] - \frac{\theta}{1 - \theta} = -\ln K_1 - \frac{K_2 \theta}{RT}, \quad (6)$$

where  $K_1$  is Hill-de Boer constant (Lm/g) and  $K_2$  is the energetic constant of the interaction between adsorbed molecules (kJ/mol). Equilibrium adsorption experiment would be studied through the plotting of  $\ln[C_e(1 - \theta)/\theta] - \theta/(1 - \theta)$  versus  $\theta$ .

## 3 Discussion and results

### 3.1 Scanning electron microscopy characterization

The variation of the morphological profile of membranes generally depends on the method of its synthesis and the technique of their exploitation [25]. The SEM micrograph and EDS of the resulted nanoparticle is shown in Fig. 2. Fig. 2(a) showed the morphological profile of the synthesized nanoparticle. The morphological profile showed spherical particles with their explicit borders and agglomerated nature and a rough surface. The image shows that the particles are very compact with tiny pores hence, exhibited a more porous surface. The medium size of the particle was measured to be about 2500 nm. This result corresponds to that found in literature from the works of Balakrishnan et al. [26]. The EDS analysis was done to make clear the elemental distribution of the synthesized MgO nanoparticle. Fig. 2(b) shows that the synthesized nanoparticle is mainly composed of magnesium with an elemental weight of 80.5%, this was as expected as the precursor compound used was magnesium nitrate. Oxygen with elemental weight of 10.0% while the elemental weight of carbon and Silicon are 6.5% and 3.0% respectively. The carbon composition of 6.5 wt% was suspected to ensue from the calcination process.

The SEM micrographs of the synthesized PET nanocomposite membranes doped with chitosan/MgO are shown in Fig. 3. The influence of the addition of MgO nanoparticles to the membrane surfaces was studied and it was observed that different homogeneous fibrous surface patterns were obtained for the three membranes with knitting views in the three images. The nanocomposite polymeric membranes show a volume dilatation. An increase in the nanoparticles added significantly stimulated the development of

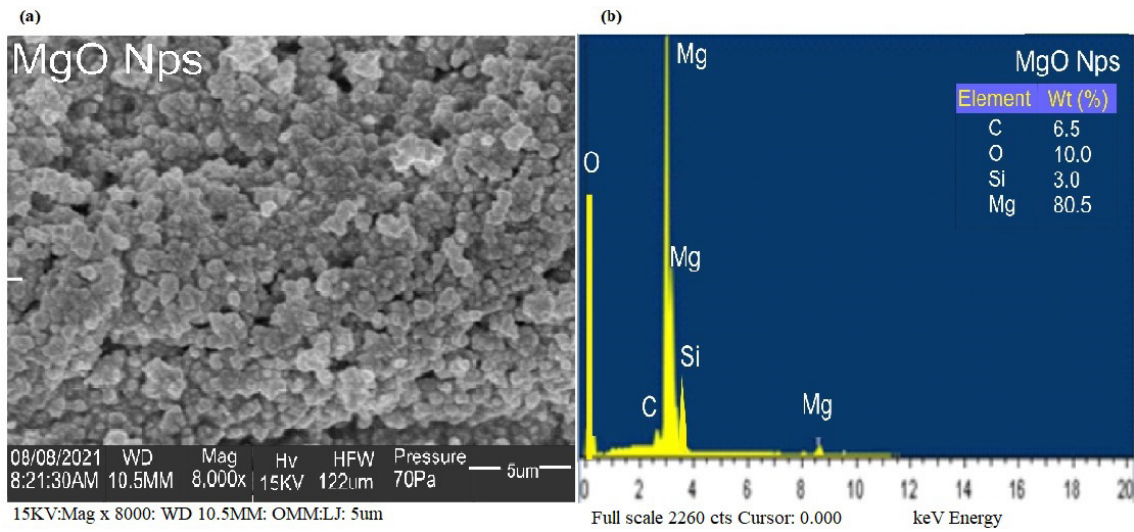


Fig. 2 SEM micrograph of (a) synthesized magnesium oxide nanoparticles; (b) EDS spectra of the synthesized magnesium oxide nanoparticles

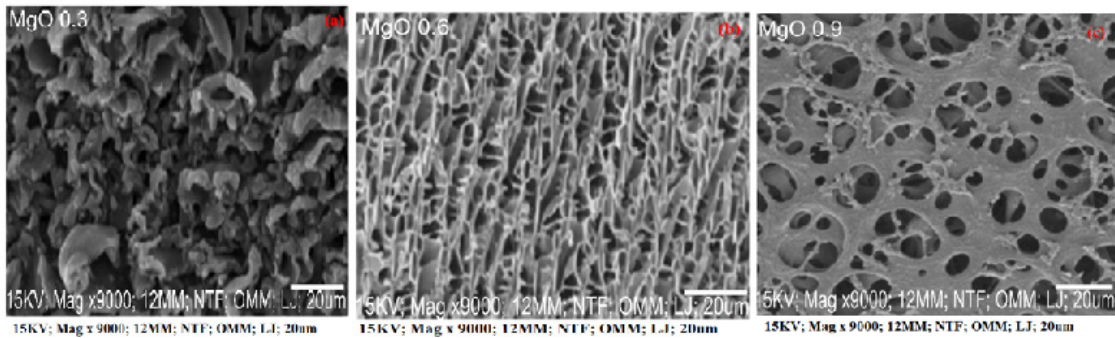


Fig. 3 SEMs micrograph of the synthesized chitosan doped magnesium oxide nanocomposite membranes (a) doped with 0.3 g MgO NP; (b) doped with 0.6 g MgO NP; (c) doped with 0.9 g MgO NP. The scale bars in the images label are 20 micrometer

aggregates of MgO on the membrane surface; which in turn formed a larger macro-voids and exhibiting finger-like structures [27–30] as a result of the volume dilatation that ensued during fabrication. The SEM images also depicted pore-like structures (nano-porosity) on the membrane surfaces; which appeared to be formed in the course of the membrane synthesis, and it was enhanced with an increase in MgO nanoparticles (Fig. 3(c)). This means that with an increase in MgO nanoparticles, the polymer nanocomposite membrane experienced larger strains, which in turn makes it energetically more favorable to accommodate volume dilatation via cavitation. In addition, the presence and stability of cavitation voids that possess sizes on the nanoscale level are connected with chain scission [31].

### 3.2 X-ray diffraction analysis

X-ray diffraction (XRD) was used to study the crystal structure of membranes and to confirm their purity and phase contents. Fig. 4 shows the characteristic peaks of the synthesized chitosan doped magnesium oxide nanocomposite

membranes. Fig. 4 compares the influence of integrating chitosan and magnesium oxide in the PET membrane. The XRD patterns of the composite membranes exhibited the presence of chitosan with broad peaks of  $19.1^\circ$  at  $2\theta$ ,

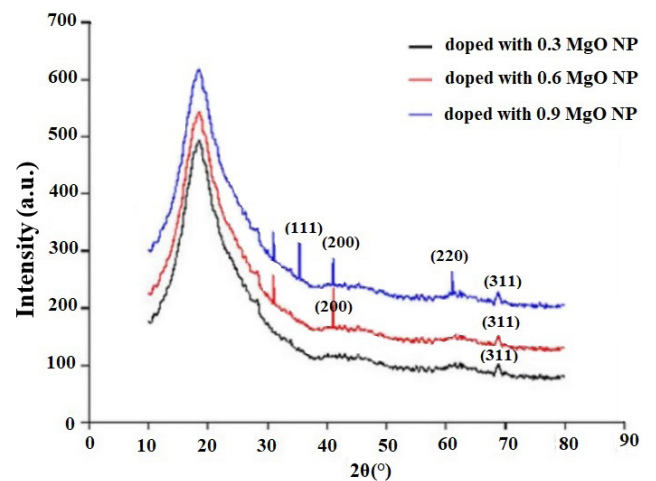
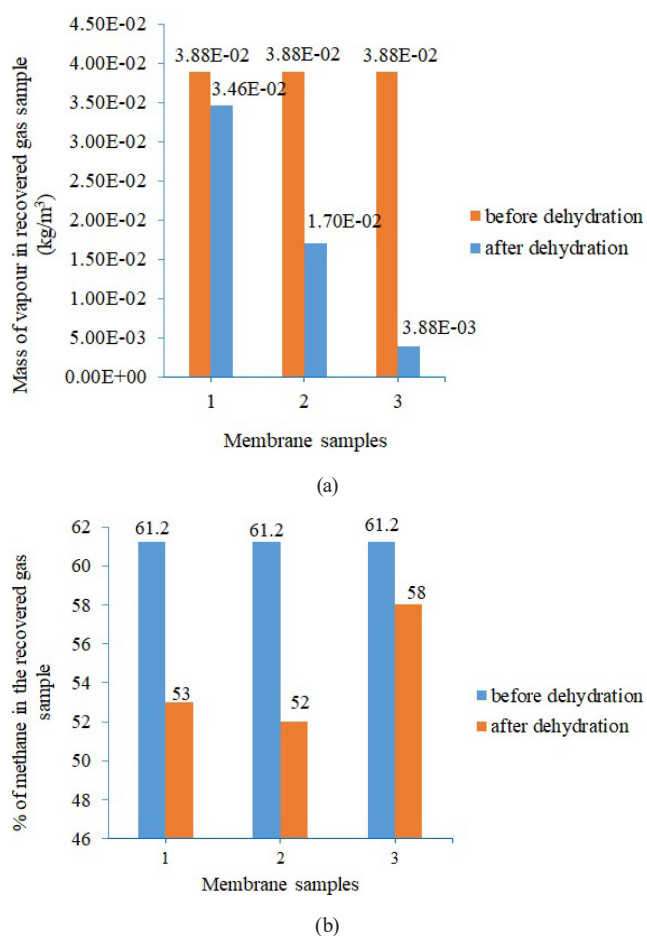


Fig. 4 X-ray diffraction spectrum of the synthesized chitosan doped magnesium oxide nanocomposite membranes

thus revealing that the composite membranes are amorphous in nature [32]. The peaks detected at (111), (200), (220) and (311) diffraction planes depict that the composite membranes exhibited a cubic phase as a result of the incorporation of MgO nanoparticles in the composite [33], at  $2\theta = 35.8^\circ$ ,  $41.5^\circ$ ,  $61^\circ$  and  $69^\circ$  respectively. The increase in peaks in Fig. 4(c) shows that the crystalline structure of the membranes increased with an increase in MgO composition. Hence, the nanocomposite membrane made of 0.9 g of MgO nanoparticle is the most crystalline since it shows the highest degree of crystallinity, while the membrane that comprises of 0.3 g of MgO is the least crystalline in nature (see Fig. 4(a)).

### 3.3 Analysis of natural gas

The analysis of the natural gas before and after dehydration of natural gas is depicted in Fig. 5. It is expected that the amount of water vapor in the residual gas will reduce and the loss of methane will be observed. Loss of methane



**Fig. 5** Gas analysis of residual gas (a) %  $\text{H}_2\text{O}$  vapor, (b) %  $\text{CH}_4$ ; of the synthesized chitosan doped magnesium oxide nanocomposite membranes (M1) doped with 0.3 MgO NP; (M2) doped with 0.6 MgO NP; (M3) doped with 0.9 MgO NP

molecules to dehydrating agent occurs during natural gas dehydration if conditions are not as optimal but the loss can be curbed. Using 0.3 g MgO-CH nanocomposite membrane, it is observed that the water vapor content in the residual gas reduced from  $3.88 \times 10^{-2}$  to  $3.46 \times 10^{-2} \text{ kgm}^3$  and methane content reduced from 61.2 to 52%. Using 0.6 g MgO-CH nanocomposite membrane, it is observed that the water vapor content in the residual gas reduced from  $3.88 \times 10^{-2}$  to  $3.17 \times 10^{-2} \text{ kgm}^3$  and methane content reduced from 61.2 to 53%. Using 0.9 g MgO-CH nanocomposite membrane, it is observed that the water vapour content in the residual gas reduced from  $3.88 \times 10^{-2}$  to  $3.88 \times 10^{-3} \text{ kgm}^{-3}$  and methane content reduced from 61.2 to 58%. This result was attained as a result of the upsurge in MgO nanoparticles coupled with the integration of chitosan during the synthesis of the membranes; consequently, there was an upsurge in permeation of the membrane and the pore size was larger thereby allowing more molecules of water vapor to pass through the membrane and reducing the adhesion of carbon from carbon-containing compounds hence reducing the methane loss. These observations can be accredited to the SEM images obtained in Fig. 3.

In addition, a coupling effect in the permeation of gas mixtures could be ensued from the interactions between permeant–permeant and the interactions between permeant–polymer [34]. Furthermore, the Fig. 5 also shows that water vapor was preferentially sorbed into the membrane with an increment of MgO, and the sorption of water can result in plasticization of the polymer matrix [34]. With regards to this study, the permeation rate of methene component in the mixture was however improved with an increase in the addition of chitosan. Nonetheless, the amount of sorbed water in the membranes restricted the available pathways of the membrane for methane to diffuse, which tends to reduce the permeation rate of methane, even with the aid of the [20]. furthermore, as a result of the strong affinity between water and the hydrophilic membrane, the presence of other gas (such as methane) in the mixture is not likely to significantly affect the water sorption and permeation [20].

### 3.4 Membrane performance for the dehydration of natural gas

Fig. 6 shows the water vapor permeability. The water vapor permeability of the nanocomposite membranes was seen to upsurge as the content of MgO NP increased. The result displayed a noteworthy water vapor permeability enhancement of 0.87 with nanocomposite membrane

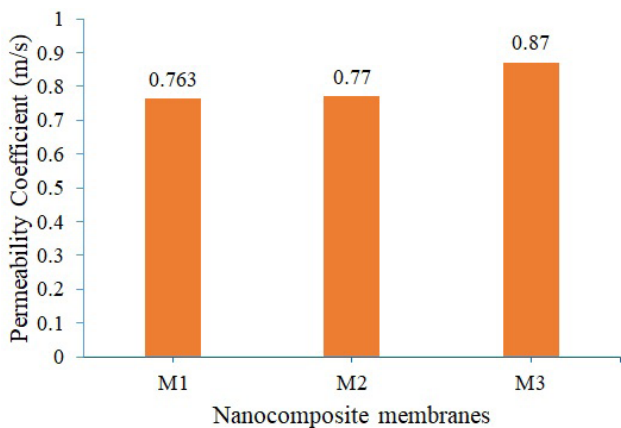


**Fig. 6** Water vapor permeability of the synthesized chitosan doped magnesium oxide nanocomposite membranes (M1) doped with 0.3 MgO NP; (M2) doped with 0.6 MgO NP; (M3) doped with 0.9 MgO NP

doped with 0.9 g MgO NP. The upsurge in water vapor permeability is in accordance with the morphological images obtained in Fig. 3. Higher content of MgO NP (0.9 g) in the casting solution resulted in the creation of larger pore sizes obtained in Fig. 3, which accelerated the transportation of water vapor across the membrane; subsequently, an upsurge in the rate of water vapor diffusion throughout the nanocomposite membrane [10]. Hence, the enhancement of the water vapor permeability from nanocomposite membrane doped with 0.3 g MgO to NP 0.6 g MgO NP to 0.9 g MgO NP. Furthermore, the upsurge in water vapor permeability ensued as a result of the upsurged interaction that takes place amid water molecules and PET agents, as a result, water solubility and permeability are anticipated to upsurge [35]. In addition, the feed water content showed negligible effect on water permeance as the permeation coefficients of the membranes are not too far from 1. Hence, the mixed-gas methane permeance was not dependent of feed water content [4].

### 3.5 Study of adsorption isotherms

Recently, many porous materials such as porous membranes have found increasing attention for the study of adsorption due to their good adsorptive properties such as the surface area, pore size, pore size distribution, and porosity, which are imperative for enhancing their use in the practical applications of nano-membranes based upon polymer blends [36]. Three adsorption isotherms were studied for the dehydration of natural gas using synthesized of PET-Magnesium oxide-chitosan nanocomposite membranes to analyze the experimental equilibrium adsorption data. The Langmuir isotherm for the adsorption of methane and vapor on the nanocomposite

membrane during dehydration is presented in Fig. 7. It was observed that the adsorbate in Fig. 7(b) got more attached to the surface of the membrane that was doped with 0.9 g MgO NP (M3); Hence the higher the quantity of MgO NP integrated into the membrane, the larger the amount of methane imprinted to the surface of the membrane. On the contrary, the higher the quantity of MgO NP integrated into the membrane, the less the vapor gets attached methane to the surface of the membrane (Fig. 7(b)). This could be due to the fact that more restrictions between the vapor and the membrane occur with the integration of a high quantity of MgO NP in the polymer matrix.

The Fowler-Guggenheim isotherm for the adsorption of methane and vapor on the nanocomposite membrane during dehydration is presented in Fig. 8. This model describes the lateral interactions between the adsorbed molecules; this indicates that there is an increase with the growing amount of CH<sub>4</sub> on the surface of the membrane integrated with 0.9 g MgO NP. At the same time, the values of Fowler-Guggenheim isotherm obtained indicate that methane molecules are adsorbed on the surface of the membrane in an ascending ordered way while water molecules are adsorbed on the surface of the membrane in a descending ordered way as the integration of the quantity of MgO increases.

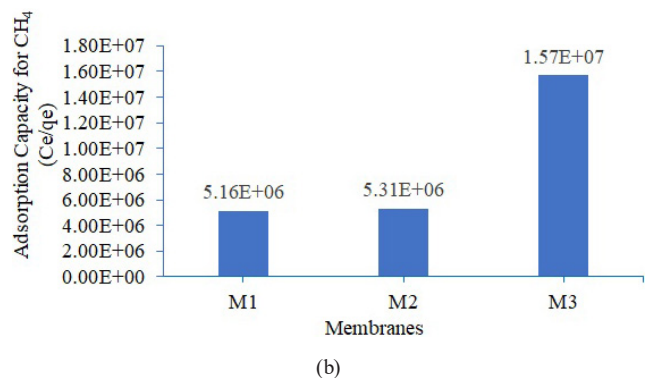
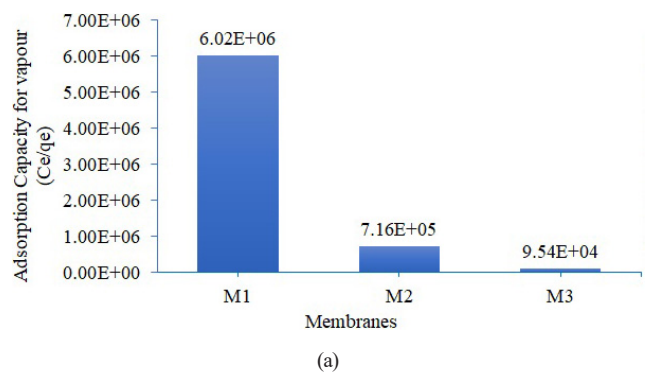
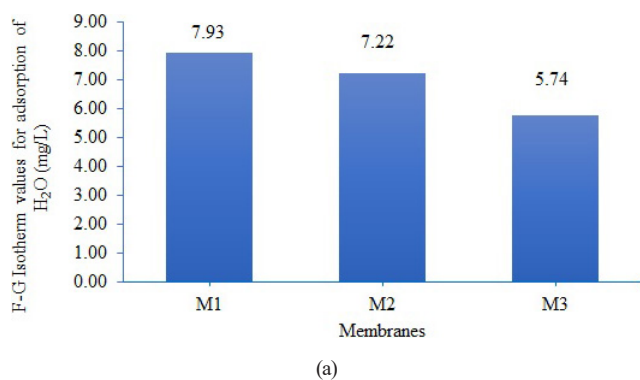
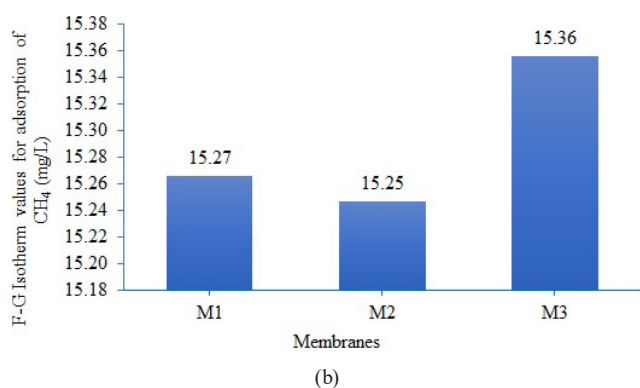


**Fig. 7** The adsorption capacity of (a) vapor and (b) methane, onto membranes using Langmuir isotherm model



(a)

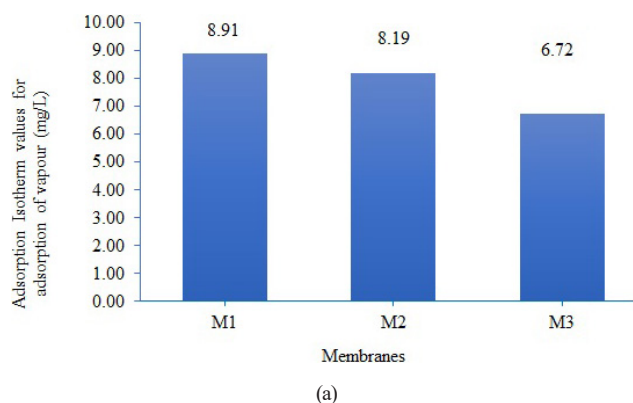


(b)

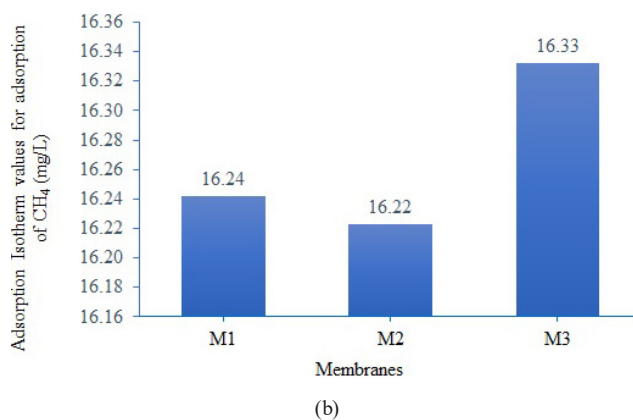
**Fig. 8** The adsorption capacity of (a) vapor and (b) methane, onto membranes using Fowler-Guggenheim (F-G) isotherm model

The Hill-de Boer isotherm equation was used to analyze the lateral adsorbate interactions and multilayer interactions. For this equation, the  $K_2$  constant is positive, which indicated interaction amid the adsorbed molecules. The Hill-de Boer isotherm for the adsorption of methane and vapor on the nanocomposite membrane during dehydration is presented in Fig. 9. It was observed that both the mobility of the adsorbed phase and adsorbate-adsorbent interactions were pronounced for CH<sub>4</sub> adsorption on the membrane, with a high quantity of MgO NP (0.9 g) in the polymer matrix, having a very high coverage (Fig. 9(b)). However, both the mobility of the adsorbed phase and adsorbate-adsorbent interactions seem to be slim with vapor adsorption on membrane, with high quantity of MgO NP (0.9 g) in the polymer matrix, at least lower coverage (Fig. 9(a)).

It is important to note that both Figs. 8 and 9 imply that some molecules of CH<sub>4</sub> and vapor were bound on the active area of the membrane as a result of the lateral adsorbate interactions and multilayer interactions between them; hence, this indicates that these models can also be used to predict the adsorption of gases onto the surface of the membranes. However, this was also at a different rate as a result of the different quantities of MgO integrated into the polymer matrix. In addition, the discrepancy in adsorption



(a)



(b)

**Fig. 9** The adsorption capacity of (a) vapor and (b) methane, onto membranes using Hill-de Boer isotherm model

between CH<sub>4</sub> and vapor in the three models is due to the different adsorption behavior of CH<sub>4</sub> and vapor on the active site of the membrane. Furthermore, higher adsorption capacity with 0.9 g MgO is due to the higher surface area of the membrane as a result of the increased quantity of MgO integrated into the membrane matrix. In addition, research has documented that the high perm selectivity to the permeation of water vapor is mainly attained from the solubility selectivity [20]. Usually, there is a positive deviation from the Henry's law with regards to sorption isotherm of vapor in polymers [20], however, different degrees of deviations was observed for the three adsorption isotherm studied.

### 3.6 Economical feasibility of making the membrane with comparison with other methods

An economic feasibility of the flat thin-film magnesium oxide-chitosan nanocomposite membrane made from PET was performed in an effort to see if it is economically feasible for a real scale system, which was also compared with other methods. The cost of making one membrane was \$38 without any inflation adjustment (see Table 3). The estimation was compared with the cost of making other membranes and other methods for dehydrating

natural gas. Table 4 shows that the flat thin-film magnesium oxide-chitosan nanocomposite membrane made from waste PET was cost effective when compared with carbon membranes [37–39]. In addition, the capital and the operating cost of the membrane system did not increase as there was no requirement of a requirement of a vacuum pump. The membrane system used the gas cylinder pressure. Following the general rules of thumb, the cost estimate for membrane system are \$500/m<sup>2</sup> membrane area for a high-pressure membrane skid [40], and \$1000/kW for a vacuum pump [9]. However, it is important to take note that carbon membrane cost may be higher compared to polymeric membranes [39]. The use of membrane system was compared with stripping water vapor from natural gas flow using triethylene glycol (TEG) in the gas dehydration process (see Table 5) [41]. It was observed that membrane system for the dehydration of natural gas using dry natural gas produced was cost effective when compared with the nitrogen gas in the dehydration package of stripping gas [41]. In Table 3, TFA represents Trifluoroacetic acid, DCM represents Dichloromethane, NaOH is Sodium

hydroxide and PEG is Polyethylene glycol. In Table 4, PET-NCM represents Polyethylene terephthalate nanocomposite membranes, w/o and w represent without and with respectively, while Ref represents the reference.

#### 4 Conclusion

The utilization of flat thin-film magnesium oxide-chitosan nanocomposite membranes was synthesized with PET and investigated for the dehydration of natural gas involving water vapor permeation. The performance of the nanocomposite membranes for gas dehydration was assessed for the different ratios of MgO nanoparticles and chitosan in the membrane matrix. The permeance of water vapor across the nanocomposite membranes was found to upsurge exponentially with an upsurge in MgO nanoparticles embedded in the membrane. The permeation coefficient increased with an upsurge MgO NP, with M1, M2 and M3 have permeation coefficient of 0.763, 0.77 and 0.87 respectively. In addition, the dehydration rate of natural gas was also found to upsurge exponentially with an upsurge in MgO nanoparticles to the PET membrane.

**Table 3** Cost analysis of fabricated membrane/m<sup>2</sup>

Raw materials	Unit price (\$/g)	Amount of raw materials used for synthesizing one membrane (g)	Cost estimated for synthesizing one membrane (\$)
Magnesium nitrate	0.34	2.97	1.0098
TFA	0.48	20	9.6
DCM	0.50	40	19.88
NaOH	0.057	2	0.114
PEG	1.85	2	3.7
Chitosan	1.315	0.2	0.263
Nonwoven polyester material	–	1	3.0662
Waste PET bottle	–	7	–
Total in dollars	–	–	\$38

**Table 4** Comparison of cost for different fabricated membranes

Types of membranes	Cost of making one membrane (\$/m <sup>2</sup> )	Ref.
Waste PET-NCM	\$38 w/o inflation	This study
Cellulose membranes	\$50 w inflation	[37]
Carbon membrane	\$100 w/o inflation	[38]
Carbon membrane	\$30–150 w/o inflation	[39]

**Table 5** Comparisons between dry natural gas produced and nitrogen gas in the dehydration package as stripping gas in regeneration column [41]

Item	Stripping in regeneration with dry natural gas	Stripping in regeneration with nitrogen	Difference between nitrogen and natural gas
Capital Cost (\$)	5,089,310	5, 149, 320	60010 (reduced)
Utility Cost (\$)	245,992	249, 424	3432 (reduced)
Purity of TEG (%)	99.7	99.7	Equal
Quantity of stripping gas (kg/h)	200.2	336.1	135.9
Vapour flow (H <sub>2</sub> O vapour + stripping gas) kg/h	701	700	1

This upsurge ensued as a result of the interaction amid the polymer chain and MgO nanoparticles together with the reduction of polymer compaction. Hence, the integration of MgO in the matrix of the membrane resulted in the formation of macro-voids on the surface of the membrane sub-layer, which in turn aided the upsurge sizes of the pores, which subsequently resulted in an upsurge in the membranes' water vapour permeability.  $3.88 \times 10^{-2} \text{ kgm}^{-3}$  gas was initially measured which reduced with an increase MgO NP, with M1, M2 and M3 having reduced the gas to  $3.46 \times 10^{-2}$ ,  $3.17 \times 10^{-2}$  and  $3.88 \times 10^{-3} \text{ kgm}^{-3}$  respectively. However, the removal of methane did not follow the same trend. There was an increase in thickness of the membrane stratum as a result of an increase in MgO incorporated into the membrane; hence, high resistance to methane

gas transport and less impact on water vapor permeability. Again, as a result of the higher permeability of water vapor in the membranes, the resistance of the dopants to water vapor permeation was significant. The difference in adsorption capacity between  $\text{CH}_4$  and vapor in Langmuir, Fowler-Guggenheim and Hill-de Boer isotherm models is due to different adsorption behavior of  $\text{CH}_4$  and vapor on the active site of the membrane. An economic evaluation of the flat thin-film magnesium oxide-chitosan nanocomposite membrane made from PET was compared with other membranes and dehydration using a stripping gas in regeneration column. The membrane used in this study was economically feasible when compared with the cost of making other membranes; as the cost of making one membrane for this study was \$38.

## References

- [1] Odunowo, T. "Natural Gas Dehydration: The Suitability of Solid Dessiccant Technology in Nigeria", In: SPE Annual Technical Conference and Exhibition, San Antonio, TX, USA, 2006, SPE-106975-STU. ISBN 978-1-55563-149-9  
<https://doi.org/10.2118/106975-STU>
- [2] Ackley, M. W., Rege, S. U., Saxena, H. "Application of natural zeolites in the purification and separation of gases", *Microporous and Mesoporous Materials*, 61(1–3), pp. 25–42, 2003.  
[https://doi.org/10.1016/S1387-1811\(03\)00353-6](https://doi.org/10.1016/S1387-1811(03)00353-6)
- [3] Kinigoma, B. S., Ani, G. O. "Comparison of Gas Dehydration Methods based on Energy Consumption", *Journal of Applied Sciences and Environmental Management*, 20(2), pp. 253–258, 2016.  
<https://doi.org/10.4314/jasem.v20i2.4>
- [4] Lin, H., Thompson, S. M., Serbanescu-Martin, A., Wijmans, J. G., Amo, K. D., Lokhandwala, K. A., Merkel, T. C. "Dehydration of natural gas using membranes. Part I: Composite membranes", *Journal of Membrane Science*, 413–414, pp. 70–81, 2012.  
<https://doi.org/10.1016/j.memsci.2012.04.009>
- [5] Ray, R. "A Membrane-Based Process for the Removal of BTEX from Glycol Dehydration Vents", EPA SBIR Phase II Project, Bend Research Inc., Washington, DC, USA, No. 68D60047, 1999.
- [6] U.S. Energy Information Administration "Country Analysis Executive Summary: Nigeria", [pdf] U.S. Energy Information Administration. Available at [https://www.eia.gov/international/content/analysis/countries\\_long/Nigeria/NigeriaCAXS\\_2020.pdf](https://www.eia.gov/international/content/analysis/countries_long/Nigeria/NigeriaCAXS_2020.pdf) [Accessed: 04 October 2021]
- [7] Mitariten, M., Mokhatab, S. "Efficient membrane systems for natural gas dehydration", *Digital Refining, Processing, Operations & Maintenance*, Sept. [online] Available at: <https://www.digitalrefining.com/article/1001543/efficient-membrane-systems-for-natural-gas-dehydration#YVr3EZpKjIU> [Accessed: 04 October 2021]
- [8] Agboola, O., Fayomi, O. S. I., Ayodeju, A., Ayeni, A. O., Alagbe, E. E., Sanni, S. E., Okoro, E. E., Moropeng, L., Sadiku, R., Kupolati, K. W., Oni, B. A. "A review on polymer nanocomposites and their effective applications in membranes and adsorbents for Water treatment and gas separation", *Membranes*, 11(2), 139, 2021.  
<https://doi.org/10.3390/membranes11020139>
- [9] Lin, H., Thompson, S. M., Serbanescu-Martin, A., Wijmans, J. G., Amo, K. D., Lokhandwala, K. A., Low, B. T., Merkel, T. C. "Dehydration of natural gas using membranes. Part II: Sweep/counter-current design and field test", *Journal of Membrane Science*, 432, pp. 106–114, 2013.  
<https://doi.org/10.1016/j.memsci.2012.12.049>
- [10] Hafani, M., Chemrak, M. A., Djennad, M., Benachour, D. "Formulation and characterization of a new PET-based membrane for methane gas dehydration", *Polymer-Plastics Technology and Materials*, 60(15), pp. 1605–1619, 2021.  
<https://doi.org/10.1080/25740881.2021.1912091>
- [11] Kleiman, S., Chaim, R. "Thermal stability of MgO nanoparticles", *Materials Letters*, 61(23–24), pp. 4489–4491, 2007.  
<https://doi.org/10.1016/j.matlet.2007.02.032>
- [12] Mohammed, M. A., Syeda, J. T. M., Wasan, K. M., Wasan, E. K. "An Overview of chitosan nanoparticles and its application in non-parental drug delivery", *Pharmaceutics*, 9(4), 53, 2017.  
<https://doi.org/10.3390/pharmaceutics9040053>
- [13] Idris, A., Mat Zain, N., Noordin, M. Y. "Synthesis, characterization and performance of asymmetric polyethersulfone (PES) ultrafiltration membranes with polyethylene glycol of different molecular weights as additives", *Desalination*, 207(1–3), pp. 324–339, 2007.  
<https://doi.org/10.1016/j.desal.2006.08.008>
- [14] Salahi, A., Mohammadi, T., Behbahani, R. M., Hemmati, M. "Experimental investigation and modeling of industrial oily wastewater treatment using modified polyethersulfone ultrafiltration hollow fiber membranes", *Korean Journal of Chemical Engineering*, 32(6), pp. 1101–1118, 2015.  
<https://doi.org/10.1007/s11814-014-0310-1>
- [15] Mulyati, S., Aprilia, S., Safiah, Syawaliah, Armando, M. A., Mawardi, H. "The effect of poly ethylene glycol additive on the characteristics and performance of cellulose acetate ultrafiltration membrane for removal of Cr(III) from aqueous solution", *IOP Conference Series: Materials Science and Engineering*, 352, 012051, 2018.  
<https://doi.org/10.1088/1757-899X/352/1/012051>

- [16] Ma, Y., Shi, F., Ma, J., Wu, M., Zhang, J., Gao, C. "Effect of PEG additive on the morphology and performance of polysulfone ultrafiltration membranes", *Desalination*, 272(1–3), pp. 51–58, 2011.  
<https://doi.org/10.1016/j.desal.2010.12.054>
- [17] Wahab, R., Ansari, S. G., Dar, M. A., Kim, Y. S., Shin, H. S. "Synthesis of magnesium oxide nanoparticles by sol-gel process", *Material Science Forum*, 558–559, pp. 983–986, 2007.  
<https://doi.org/10.4028/www.scientific.net/MSF.558-559.983>
- [18] De Silva, R. T., Mantilaka, M. M. M. G. P. G., Ratnayake, S. P., Amaratunga, G. A. J., Nalin de Silva, K. M. "Nano-MgO reinforced chitosan nanocomposites for high performance packaging applications with improved mechanical, thermal and barrier properties", *Carbohydrate Polymers*, 157, pp. 739–747, 2017.  
<https://doi.org/10.1016/j.carbpol.2016.10.038>
- [19] Dongre, R. S. "Marine Polysaccharides in Medicine", In: Shalaby, E. (ed.) *Biological Activities and Application of Marine Polysaccharides*, IntechOpen, 2017, pp. 181–206. ISBN 978-953-51-2859-5  
<https://doi.org/10.5772/62752>
- [20] Du, J. R., Liu, L., Chakma, A., Feng, X. "Using poly(N,N-dimethylaminoethyl methacrylate)/polyacrylonitrile composite membranes for gas dehydration and humidification", *Chemical Engineering Science*, 65(16), pp. 4672–4681, 2010.  
<https://doi.org/10.1016/j.ces.2010.05.005>
- [21] Elmorsi, T. M. "Equilibrium isotherms and kinetic studies of removal of methylene blue dye by adsorption onto miswak leaves as a natural adsorbent", *Journal of Environmental Protection*, 2(6), pp. 817–827, 2011.  
<https://doi.org/10.4236/jep.2011.26093>
- [22] Dąbrowski, A. "Adsorption - from theory to practice", *Advances in Colloid and Interface Science*, 93(1–3), pp. 135–224, 2001.  
[https://doi.org/10.1016/S0001-8686\(00\)00082-8](https://doi.org/10.1016/S0001-8686(00)00082-8)
- [23] Ayawei, N., Ebelegi, A. N., Wankasi, D. "Modelling and interpretation of adsorption isotherms", *Journal of Chemistry*, 2017, 3039817, 2017.  
<https://doi.org/10.1155/2017/3039817>
- [24] Kumar, P. S., Ramalingam, S., Kirupha, S. D., Murugesan, A., Vidhyarevi, T., Sivanesan, S. "Adsorption behavior of Nickel(II) onto cashew nut shell: Equilibrium, thermodynamics, kinetics, mechanism and process design", *Chemical Engineering Journal*, 167(1), pp. 122–131, 2010.  
<https://doi.org/10.1016/j.cej.2010.12.010>
- [25] Berradi, M., Berradi, O., Chellouli, M., Hsissou, R., El Bouchti, M., El Gouri, M., Sallek, B., El Bachiri, A., El Harfi, A. "Optimization of the synthesis of ultrafiltration asymmetric membranes based on organic polymers", *Results in Engineering*, 6, 100116, 2020.  
<https://doi.org/10.1016/j.rineng.2020.100116>
- [26] Balakrishnan, G., Velavan, R., Mujasam Batoo, K., Raslan, E. H. "Microstructure, optical and photocatalytic properties of MgO nanoparticles", *Results in Physics*, 16, 103013, 2020.  
<https://doi.org/10.1016/j.rinp.2020.103013>
- [27] Hassan, A. R., Rozali, S., Safari, N. H. M., Besar, B. H. "The roles of polyethersulfone and polyethylene glycol additive on nanofiltration of dyes and membrane morphologies", *Environmental Engineering Research*, 23(3), pp. 316–322, 2018.  
<https://doi.org/10.4491/eer.2018.023>
- [28] Safari, N. H. M., Hassan, A. R., Che Wan Takwa, C. W. I., Rozali, S. "Deduction of Surfactants Effect on Performance, Morphology, Thermal and Molecular Properties of Polymeric Polyvinylidene Fluoride (PVDF) Based Ultrafiltration Membrane", *Periodica Polytechnica Chemical Engineering*, 63(1), pp. 27–35, 2019.  
<https://doi.org/10.3311/PPch.12423>
- [29] Hassan, A. R., Che Wan Takwa, C. W. I., Mohd Safari, N. H., Rozali, S., Sulaiman, N. A. "Characterization on Performance, Morphologies and Molecular Properties of Dual-Surfactants Based Polyvinylidene Fluoride Ultrafiltration Membranes", *Periodica Polytechnica Chemical Engineering*, 64(3), pp. 320–327, 2020.  
<https://doi.org/10.3311/PPch.13862>
- [30] Rozali, S., Safari, N. H. M., Hassan, A. R., Ahmad, M., Yunus, R. M. "Assessment on Performance-properties of Asymmetric Nanofiltration Membranes from Polyethersulfone/n-Methyl-2-pyrrolidone/water Blends with Poly(vinyl pyrrolidone) as Additive", *Periodica Polytechnica Chemical Engineering*, 66(1), pp. 54–69, 2022.  
<https://doi.org/10.3311/PPch.18357>
- [31] Michler, G. H., von Schmeling, H.-K. K.-B. "The physics and micro-mechanics of nano-voids and nano-particles in polymer combinations", *Polymer*, 54(13), pp. 3131–3144, 2013.  
<https://doi.org/10.1016/j.polymer.2013.03.035>
- [32] Nga, N. K., Thuy Chau, N. T., Viet, P. H. "Preparation and characterization of a chitosan/MgO composite for the effective removal of reactive blue 19 dye from aqueous solution", *Journal of Science: Advanced Materials and Devices*, 5(1), pp. 65–72, 2020.  
<https://doi.org/10.1016/j.jsamd.2020.01.009>
- [33] Ashok, C. H., Venkateswara Rao, K., Shilpa Chakra, C. H. "Synthesis and Characterization of MgO/TiO<sub>2</sub> Nanocomposites", *Journal of Nanomedicine & Nanotechnology*, 6(6), 1000329, 2015.  
<https://doi.org/10.4172/2157-7439.1000329>
- [34] Zhu, W., Gora, L., van de Berg, A. W. C., Kapteijn, F., Jansen, J. C., Moulijn, J. A. "Water vapour separation from permanent gases by a zeolite-4A membrane", *Journal of Membrane Science*, 253(1–2), pp. 57–66, 2005.  
<https://doi.org/10.1016/j.memsci.2004.12.039>
- [35] Zare, B., Ameri, E., Sadeghi, M. "Dehydration of natural gas using polyether sulfone (PES) membrane and its nanocomposite with silica particles and nitrogen sweeping gas", *Chemical Methodologies*, 5(4), pp. 308–316, 2021.  
<https://doi.org/10.22034/CHEMM.2021.131096>
- [36] Agboola, O., Sadiku, E. R., Mokrani, T. "Chapter 6 - Nanomembrane Materials Based on Polymer Blends", In: Thomas, S., Shanks, R., Chandrasekharakurup, S. (eds.) *Design and applications of nanostructured polymer blends and nanocomposite systems: A volume in Micro and Nano Technologies*, William Andrew, 2016, pp. 101–123. ISBN 978-0-323-39408-6  
<https://doi.org/10.1016/B978-0-323-39408-6.00006-6>
- [37] He, X., Chu, Y., Lindbråthen, A., Hillestad, M., Hägg, M.-B. "Carbon molecular sieve membranes for biogas upgrading: Techno-economic feasibility analysis", *Journal of Cleaner Production*, 194, pp. 584–593.  
<https://doi.org/10.1016/j.jclepro.2018.05.172>

- [38] Chu, Y., He, X. "Process Simulation and Cost Evaluation of Carbon Membranes for CO<sub>2</sub> Removal from High-Pressure Natural Gas", *Membranes*, 8(4), 118, 2018.  
<https://doi.org/10.3390/membranes8040118>
- [39] He, X., Kumakiri, I., Hillestad, M. "Conceptual process design and simulation of membrane systems for integrated natural gas dehydration and sweetening", *Separation and Purification Technology*, 247, 116993, 2020.  
<https://doi.org/10.1016/j.seppur.2020.116993>
- [40] Baker, R. W., Lokhandwala, K. "Natural gas processing with membranes: an overview", *Industrial & Engineering Chemistry Research*, 47(7), pp. 2109–2121, 2008.  
<https://doi.org/10.1021/ie071083w>
- [41] Gad, M. S., Elmawgoud, H. A., Aboul-Fotouh, T. M., El-Shafie, M. A. "The economic comparison between dry natural gas and nitrogen gas for stripping water vapor from glycol in the gas dehydration process", *International Journal of Engineering Science Invention*, 5(8), pp. 8–12, 2016.